Cellulose (2022) 29:6231–6245
https://doi.org/10.1007/s10570-022-04656-w

ORIGINAL RESEARCH

Alginate modified graphene oxide for rapid and effective sorption of some heavy metal ions from an aqueous solution

A. I. Abd-Elhamid · E. M. Abu Elgoud · H. F. Aly

Received: 2 March 2022 / Accepted: 17 May 2022 / Published online: 9 June 2022

Abstract Herein, we investigated a new strategy to modify the graphene oxide (GO) with sodium alginate (SA) using tetraethylorthosilicate (TEOS) as a binding agent. The graphene oxide-sodium alginate composite was highly loaded with carboxylate ($-COO^{-}Na^{+}$) groups, which permitted fast and efficient interaction with the metal ions. Therefore, the prepared composite was employed as an efficient adsorbent to uptake some heavy metals from an aqueous solution. The as-synthesized GO-SA was characterized by various advanced techniques before and after the removal process. The analysis of the experimental data showed that the Langmuir model fits well the adsorption data with maximum adsorption capacities of 887.21, 161.25, and 139.62 mg g^{-1} for Pb^{2+}, Zn^{2+}, and Cd^{2+}, respectively. Moreover, the GO-SA presented a good regeneration and reuse ability, enhancing the removal rate for all the studied metal ions. In addition, the prepared composite showed a suitable selectivity for Pb^{2+} from Zn^{2+}, and Cd^{2+} co-existed solution.

Keywords Graphene oxide · Sodium alginate · Contaminants removal · Heavy metal · Regeneration · Selectivity

Introduction

Nuclear fuel cycle creates extensive amounts of aqueous waste solutions polluted with different heavy metals. Some toxic heavy metals like zinc (Zn^{2+}), lead (Pb^{2+}), and cadmium (Cd^{2+}) cause serious and toxic effects on the living environment. Cd^{2+}, Zn^{2+}, and Pb^{2+} ions exist in industrial and radioactive waste. Cd has various radioisotopes, among which ^{109}Cd with a half-life of 462.9 days. It is applied in nuclear reactors as control rods and shields to absorb neutrons (Aglan et al. 2014). It also has an important role in producing nickel–cadmium (Ni–Cd) rechargeable batteries and has been used as a corrosion-protection coating for iron and steel. General industrial uses for cadmium, include alloys, batteries, solar cells, pigments, coatings (electroplating), and plastic stabilizers (Carolin et al. 2017a, b). Zinc presents in wastewater streams generated from many industries, such as steel works, the electroplating process, and intermediate-level active waste (Ali and Ache 1985).

Supplementary Information The online version contains supplementary material available at https://doi.org/10.1007/s10570-022-04656-w.

A. I. Abd-Elhamid (✉)
Composites and Nanostructured Materials Research Department, Advanced Technology and New Materials Research Institute, City of Scientific Research and Technological Applications (SRTA-City), New Borg Al-Arab, Alexandria 21934, Egypt
e-mail: ahm_ch_ibr@yahoo.com

E. M. A. Elgoud · H. F. Aly
Hot Laboratories Center, Egyptian Atomic Energy Authority, Cairo 13759, Egypt

Adding Zn to nuclear reactors greatly reduces corrosion processes, including stress corrosion cracking. Lead is highly toxic and can harm the nervous system and kidneys. Pb^{2+} has several sources, including effluents from battery manufacturing, painting pigment, steel industries, fuel production, coating industries, and explosive manufacturing. Since Pb^{2+} effectively absorbs electromagnetic radiation of short wavelengths, it is utilized as a protective shielding around nuclear reactors for gamma rays, particle accelerators, and X-ray equipment. It is also used as containers for transporting and storing radioactive materials (Dodd 2020). Numerous trials were carried out to remove various heavy metal ions from the aqueous solution using the adsorption approach. Rodríguez et al. (2020) studied the removal of aluminum (Al) and copper (Cu) from acid mine drainage wastewater. They found that the decoration of GO with zinc oxide (ZnO) nanoparticles can remove the Al and Cu from acidic water (pH 4) with an adsorption capacity of 19.9 mg g^{-1} for Al^{3+} and 33.5 mg g^{-1} for Cu^{2+} over 30 min. Katubi et al. (2021) successed in adsorption of 636.94 mg g^{-1} of Pb-ion onto $MnFe_2O_4$/GO composite at pH 7, and the optimum contact time was 30 min. Li et al. (2020) investigated the preparation of graphene oxide/chitosan (GO/CS) complex and its behavior for adsorption of Cu^{2+}, Pb^{2+}, and Cd^{2+} ions from simulated wastewater. Their results showed that the one gram of GO/CS composite could adsorb 60.7 mg of Cu^{2+}, 48.7 mg of Pb^{2+}, and 32.3 mg of Cd^{2+} at a time of 90 min and pH 6. Pourbeyram (2016) studied the modified GO surface with zirconium and phosphate to synthesize graphene oxide–zirconium phosphate (GO-Zr-P) nanocomposite. He observed that the prepared composite (GO-Zr-P) could achieve maximum adsorption capacity for Pb^{2+} (363.42 mg g^{-1}), Cd^{2+} (232.36 mg g^{-1}), Cu^{2+} (328.56 mg g^{-1}), and Zn^{2+} (251.58 mg g^{-1}) at pH 6 and after 20 min contact time. Removal of Pb^{2+} from aqueous solution using a nanocomposite of ZnO/GO has been investigated by Ahmad et al. (2020). They reported that at pH 5 and after 160 min mixing time, the ZnO/GO possessed a maximum adsorption capacity of 418.78 mg g^{-1} for Pb^{2+}. Bagheri et al. (2020) evaluated the prepared rGO-Fe^0/Fe_3O_4-PEI nanocomposite for Pb^{2+} and Cd^{2+} removal. Their findings showed that the maximum adsorption capacity reached 60.24 mg g^{-1} for Pb^{2+} and 54.47 mg g^{-1} for Cd^{2+} at pH 6 and 60 min of contact time. Kong et al. (2020) studied the adsorption of Pb^{2+} and Cu^{2+} on GO-terminated hyperbranched amino polymer-carboxymethyl cellulose ternary nanocomposite (GO-HBP-NH_2-CMC). They reported that the maximum adsorption capacity of GO-HBP-NH_2-CMC towards Pb^{2+} is 152.86 mg g^{-1} and Cu^{2+} 137.48 mg g^{-1} at pH 5 and mixing time 240 min. Removal of Pb^{2+} has been studied by partially r-GO-Fe_3O_4 composite from aqueous solutions by Guo et al. (2018). They found that one gram of the nano adsorbent can interact with 373.14 mg of Pb^{2+} at pH 6 within 10 min. Yang et al. (2020) employed the oily sludge pyrolysis residue for decontaminating the heavy metal from synthetic flotation wastewater. The experimental results showed that the maximum uptake of the used adsorbent for Cd^{2+} (106.16 mg g^{-1}), Pb^{2+} (140.65 mg g^{-1}), and Cu^{2+}(128.04 mg g^{-1}) at pH < 7.5 and contact time 45 min. Ge and Ma (2015) used microwave irradiation to fabricate triethylenetetramine-modified graphene oxide/chitosan (TGOCS). The affinity of TGOCS towards Cr^{6+} from the aqueous solution was 219.5 mg g^{-1}.

Sodium alginate (SA) is an anionic linear polysaccharide based on alternating blocks of β-(1 → 4)-linked D-mannuronic acid (M) and α-(1 → 4)-linked L-guluronic (G) residues. With a high density of free hydroxyl and carboxyl groups located over the alginate backbone, these make the SA highly reactive and amenable to chemical modifications and complexation. On the other hand, the GO was found as nanosheets with one C-atom thickness and various O-function groups distributed over the GO nanosheet surface. Several studies were investigated in order to combine the GO and SA; Yu et al. (2019) prepared hydrogel beads composed of polyvinyl alcohol (PVA)/GO-SA via crosslinking in a saturated solution of saturated boric acid and $CaCl_2$. They observed that PVA and SA molecules were bonded with GO layers via H-bond, which causes significate disorder in the layered structure of GO. In addition, with the increase in the GO dose, the hydrogel beads lose their ballbility and network structure, enhancing their permeability and adsorption capacity towards Pb^{2+} (279.43 mg g^{-1}). Yu et al. (2021) employed the vacuum filtration technique to fabricate a self-support composite membrane formed from GO/SA/1, 2-Propanediamine (PDA) for adsorption of Pb^{2+}. The adsorption experiments revealed that the equilibrium adsorption was reached after 20 min.

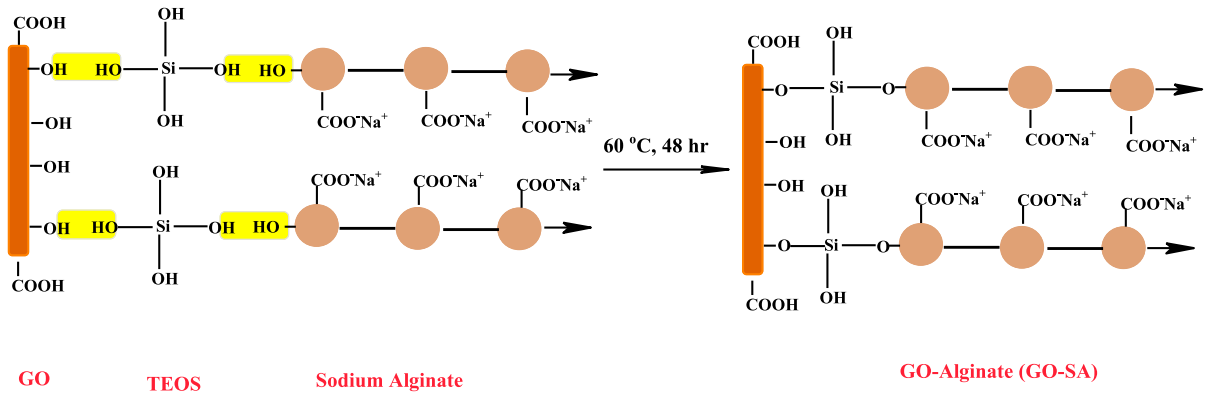

Scheme 1 The schematic preparation of GO-SA adsorbent

Moreover, according to Langmuir, the maximum adsorption capacity for Pb^{2+} was 189.25 mg g^{-1}. He et al. (2020) investigated a novel hydrogel adsorbent consisting of yttrium-immobilized-graphene oxide-alginate (Y-GO-SA) for removal of adsorption of As^{5+} and tetracycline (TC). The adsorption process was pH-dependent. The maximum adsorption capacities obtained were 273.39 mg g^{-1} (As^{5+}) and 477.9 mg g^{-1} (TC). Jiao et al. (2016) prepared a porous aerogel structure from sodium alginate/graphene oxide (SA/GO) using an in-situ crosslinking and freeze-drying strategy. As a reinforcing filler, the addition of GO enhances various properties of the obtained SAGO aerogel, such as porous structure, mechanical strength, elasticity, and compression strength. Refer to the Langmuir isotherm, the maximum removing capacities for Cu^{2+} (98.0 mg g^{-1}) and Pb^{2+} (267.4 mg g^{-1}). Zhou et al. (2018) employed the hydrothermal polymerization of lignin, SA, and GO in an aqueous solution to form 3D porous composite (PG/L/SA). The results obtained from the adsorption experiments showed that the PG/L/SA achieved maximum adsorption ability of Cd^{2+} and Pb^{2+} of 79.88 and 226.24 mg g^{-1}, respectively. Pan et al. (2018) used a sacrificial template of polystyrene particles to form porous calcium alginate/graphene oxide composite aerogel (mp-CA/GO). They observed that the (mp-CA/GO) possess suitable adsorption capacities towards Pb^{2+} (368.2 mg g^{-1}), Cu^{2+} (98.1 mg g^{-1}), and Cd^{2+} (183.6 mg g^{-1}), and adsorption equilibrium achieved after 40 min.

Based on the abovementioned information, the scientists used various strategies to prepare the GO/SA hydrogel (porous structure, beads, layer, aerogel, etc.). The preparation of these composites required multi-steps. Moreover, a part of the bind sites was consumed by crosslinking or shieling interior in the bulk gel. As a result, the time for reaching equilibrium will be elongated, and the adsorption capacity will be reduced.

In this work, a modification of the GO surface with SA using TEOS as a bridge to link the hydroxyl groups of GO and SA was suggested. This manner will provide an extra and efficient binding site ($–COO^{-}Na^{+}$) available for highly rapid chelating of the heavy metal ion. The as-prepared GO-SA composite was characterized by different techniques and applied to remove Pb^{2+}, Zn^{2+}, and Cd^{2+} from the aqueous solution using the batch technique.

Experimental

Materials and instrumentation

See supplementary materials.

Preparation of GO and GO-SA composite

The GO was synthesized according to our previous strategy (Abd-Elhamid et al. 2018). The GO-SA was fabricated via a simple mixing approach, see Scheme 1. In detail, 4 g of SA was added to 1000 mL distilled water under stirring until the solution became clear. Thereafter, GO (0.15 g) was appended to the alginate solution at constant stirring to form a

homogeneous GO-alginate suspension solution (a). In another beaker, an alcoholic solution of TEOS was prepared separately by adding 5 mL TEOS to 25 mL absolute ethanol solution (b). Then, solution (b) was drop-wisely added to the solution (a), and the final solution was kept stirring for 48 h at 60 °C. The resulted viscous solid was separated by filtration, washed several times with distilled water, and stored for further use.

Batch adsorption of heavy metals

A stock solution of 1000 mg L^{-1} was prepared by dissolving proper amounts of every metal ion in double-distilled water. A batch sorption experiments were conducted in order to study the parameters that affect the sorption of Pb^{2+}, Cd^{2+} and Zn^{2+}, such as shaking time, pH, v/m, initial metal concentration, and temperature, where the optimized conditions were determined and repeated three times. A 2.8 mg of GO-SA was added to glass bottles containing 5 mL of definite concentrations of Pb^{2+}, Cd^{2+}, and Zn^{2+}, then mixed and shaken in a thermo-stated shaker bath adjusted at 25 °C. The pH values were adjusted by adding a 0.1 mmol solution of HNO_3 or NaOH. Different parameters were investigated, including the effect of shaking time (1–30 min), pH (1–8), initial metal ion concentration (25–150 mg L^{-1}) for Cd^{2+} and Zn^{2+}, (200–1000 mg L^{-1}) for Pb^{2+}, and temperature (25–65 °C). The metal concentration was spectrophotometrically determined with a Shimadzu double beam spectrophotometer using 4-(pyridyl-2-azo) resorcinol (PAR) (Marczenko 1976). Batch experiments were done by shaking 2.8 mg of the prepared graphene oxide alginate with 5 mL of the metal ions solution in a thermo-stated shaker bath adjusted at 25 °C to achieve an adsorption equilibrium condition. This process was repeated three runs and the average value was used as the M-ion concentration in the aqueouse solution. The removal percentage (R%) of Pb^{2+}, Cd^{2+}, and Zn^{2+} at equilibrium was calculated, as given in Eq. 1.

$$R\% = \left(\frac{C_o - C_e}{C_o}\right) * 100 \quad (1)$$

where C_o and C_e are the initial and equilibrium concentrations (mg L^{-1}) of the metal ions in solution, respectively.

Characterization

See supplementary materials.

Adsorption kinetics study

See supplementary materials.

Adsorption isotherm

See supplementary materials.

Thermodynamic study of adsorption

See supplementary materials.

Results and discussion

Characterization

TEM and SEM

The TEM images of the GO layer appear as a single and highly transparent sheet (Abd-Elhamid et al. 2018). After modification of the GO surface with alginate, the GO-SA composite layer appears to be dusk and cloudy, see Fig. 1a–c, which may be due to the modification with alginate. The volume of Fig. 1c was increased (see Fig. S1) to clearly demonstrate the layered structure of the composite.

The morphological structure of the GO-SA composite was determined with the SEM technique. Figure 1d–h presents the SEM photographs of the GO-SA at various magnifications. At low magnifications, the composite appears as fully separated distributed particles, as shown in Fig. 1d. Moreover, the volume of the image (Fig. 1d) is enlarged, and the limits of GO-SA composite layers were detected with red arrows, as seen in Fig. 2S. With the increase in the magnification power, the layered structure became clearer, and cracks appeared on the composite surface, Fig. 1e, f. At higher magnification, the cracks could be detected clearly in a separated bulky structure, which may refer to the dried SA that coated the GO surface Fig. 1g, h.

However, the morphology of the composite was different after the adsorption of the metal ions, see Fig. S3. Moreover, the resulted composite-metal

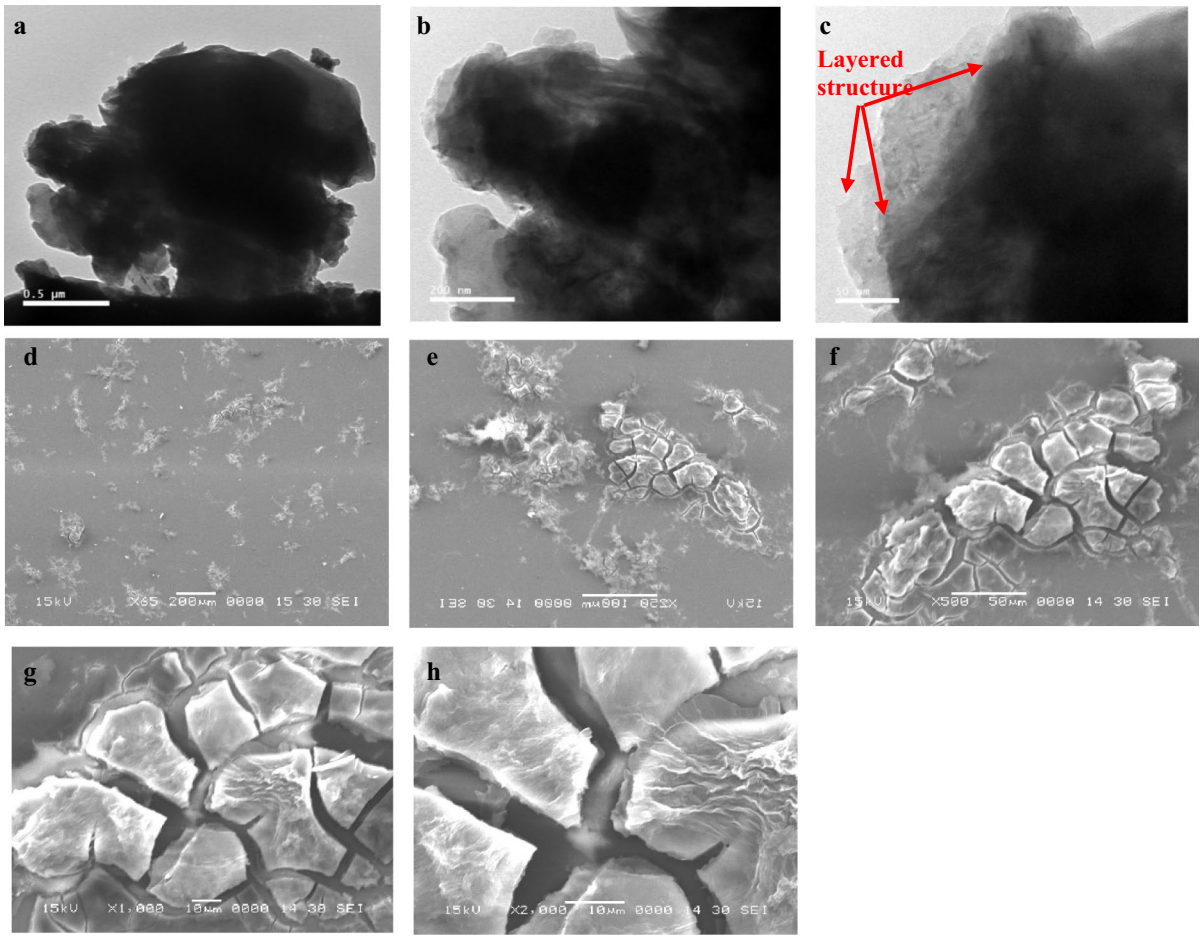

Fig. 1 TEM (**a**–**c**) and SEM (**d**–**h**) images for alginate modified graphene oxide (GO-SA)

(GO-SA-M) morphological structure depends on the type of the adsorbed metal ions. After adsorption of Pb-ions, the GO-SA-Pb complex seems like layers with particles deposited on its surface. While in the case of adsorption of Cd-ions, the structure of the GO-SA-Cd complex is not greatly altered from the original composite. Moreover, at adsorbing of Zn-ions, the yielded GO-SA-Zn complex looks alike a great agglomerated bulky structure. The alteration of the morphological structure of the composite after the adsorption process may indicate that the adsorption of the selected metal ions is by crosslinking adsorption mechanism.

FTIR

The chemical structure of the GO and modified GO (GO-SA) were characterized by the FTIR spectra (Fig. 2a). The GO possessed bands were typically observed in our previous work (Abd-Elhamid et al. 2018) at 3433 cm^{-1}, 1635 cm^{-1}, 1398 cm^{-1}, and 1033 cm^{-1}, referring to O–H stretching, O–H bending, and COOH and C–O stretching, respectively (Febrianastuti et al. 2019).

After modification of GO by the alginate and TEOS as a crosslinker, the GO-SA showed bands at 3434 cm^{-1} (adsorbed water and O–H

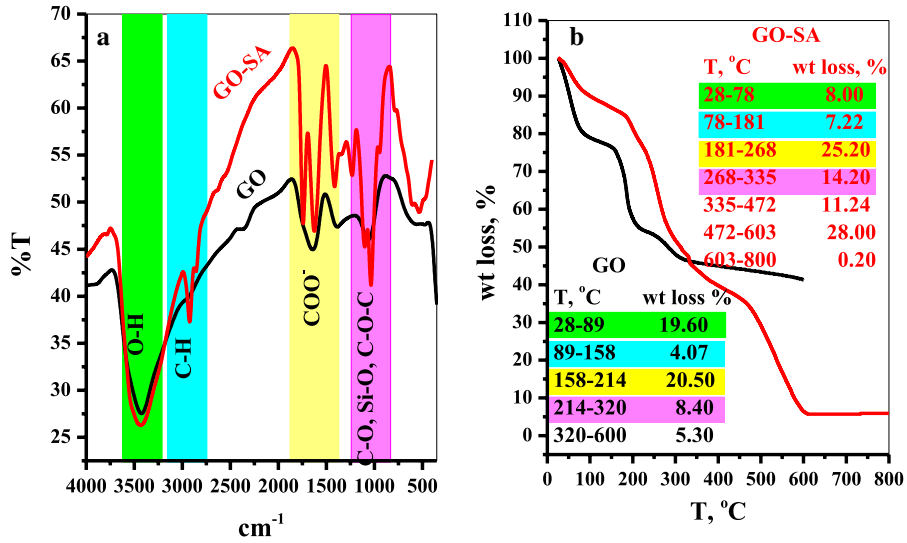

Fig. 2 **a** FT-IR spectrum of GO and GO-SA composite and **b** Thermogravimetric diagram of GO and GO-SA composite

stretching), 2923 cm^{-1} (CH_2 group), bands at 1740 and 1347 cm^{-1} belongs to vibration modes of C–O bond related to the COOH groups. The peaks at 1625 and 1413 cm^{-1} correspond to the asymmetric and symmetric stretching modes of carboxylate salt groups (–COONa), respectively (Nigiz 2020). The peaks in rang 1100–1000 cm^{-1} assigned to the (C–O, Si–O, and C–O–C stretching) of the GO, TEOS, and glycoside bonds in the polysaccharide, respectively (Fig. 2a). This big difference in the FTIR spectra between the GO and GO-SA may be affirmed the modification process.

After adsorption of metal ions, FTIR spectra of GO-SA-M (M = Pb^{2+}, Cd^{2+} or Zn^{2+}) complexes differed from the GO-SA spectrum. Where the intensity of the bands in the region 1740–1100 highly weaken (Allouss et al. 2020). These observations may be due to the complexation interaction between the various functional groups of the GO-SA composite and the M-ions (Cui et al. 2015), see Fig. S4.

TGA

Thermogravimetric analysis of the GO and GO-SA composite was investigated to detect the influence of the modification step on the thermal properties of the prepared composite. The TGA graph of the GO and GO-SA composite was presented in Fig. 2b. As obtained in our previous research (Abd-Elhamid et al. 2018), four degradation steps were presented for GO decomposition (Fig. 2b), namely, (i) liberation of the surface moisture evaporation (19.6%) at a temperature of 28–88 °C, (ii) releasing of adsorbed water (4.07%) at 88–158 °C, (iii) decomposition of oxygenated function groups –OH and C–O–C (20.50%) at 158–215 °C, and (iv) pyrolysis of –COOH at 215–320 °C, see Fig. 2b.

On the other hand, upon linking the GO with alginate via silane bonding, the thermal characters of the synthesized composite (GO-SA) extremely differed from that related to the GO. The thermograph for GO-SA showed seven pyrolysis stages, as illustrated in Fig. 2b. Therefore, the existence of the alginate assembled on the GO-surface minimized the quantity of the adsorbed moisture and bounded surface water. Where the GO-SA release 8.00% moisture at temperature (78 °C), which is lower than that of the GO, see Fig. 2b. This phenomenon is due to the functionalization process consumes the hydroxyl (–OH) on the GO surface. These (OH) groups were the responsible for bounding with high moisture amounts via H-bonding. Moreover, the partial ionic bond between the Na-ion of the alginate carboxylic group will attract low amounts of moisture molecules. On the other hand, the amount of intermolecular water by the GO-SA (7.22%), which evaporated at T = 181 °C, was larger than that shown for GO (Fig. 2b). This may be attributed to the properties of the alginate hydrogel to retain extra water molecules within its chain, which require a higher temperature to release them (Ablouh et al. 2019; Gopalakannan et al. 2016).

Moreover, Liu et al. (2015a, b) demonstrated that SA started to decompose from 202 to 289 °C; this might be referred to the break of glycosidic bonds, dehydration, decarboxylation, and decarbonylation of the alginate. Herein, GO-SA composite smoothy degrades, and its weight is reduced by 25.20% at 181–268 °C, 14.20% at 268–335 °C, 11.24% at 335–472 °C, and 28.00% at 472–603 °C. This behavior may be ascribed as the alginate chains modified the GO freely extend in the space, and these chains gradually pyrolyzed. Moreover, the alginate chains may be crosslinked with a silane linker, this will enhance the thermal properties of the prepared composite.

EDS analysis

The EDS is an important device required to detect the elements related to the prepared sample. The TEM-EDS mapping of the GO-SA composite showed that the GO-SA composite is composed of C, O, Si, and Na elements, and these elements are homogeneously

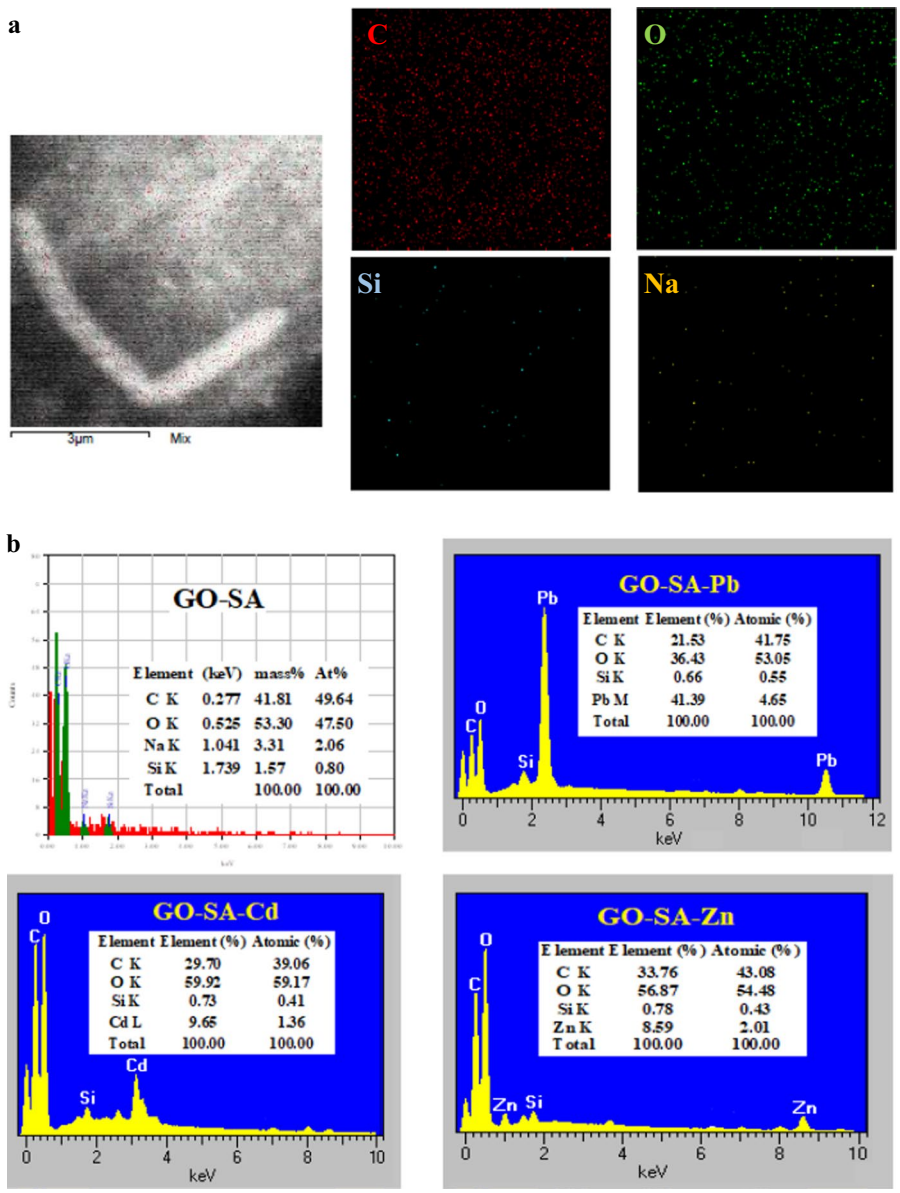

Fig. 3 **a** TEM- EDS mapping of GO-SA and **b** SEM–EDS analysis for GO-SA composite, GO-SA-Pb complex, GO-SA-Cd complex and GO-SA-Zn complex

distributed over the analyzed area, as presented in Fig. 3a.

The use of SEM–EDS for analysis of the composite (GO-SA) that was prepared by employing GO, SA, and TEOS, confirmed the presence of C, O, Si, and Na atoms in the analyzed sample. By blending the composite materials with the M-ion (Pb, Cd, and Zn) solutions. The EDS analysis detected the appearance of Pb, Cd, and Zn and the absence of Na in the analysis data of the analyzed samples. These results confirm that the adsorption process proceeded through the cation exchange mechanism, Fig. 3b.

Adsorption experiments

Effect of contact time

The relation between removal percent (%R) against contact time is illustrated in Fig. 4a. From this figure, it is clear that the removal percent (%R) is quite fast

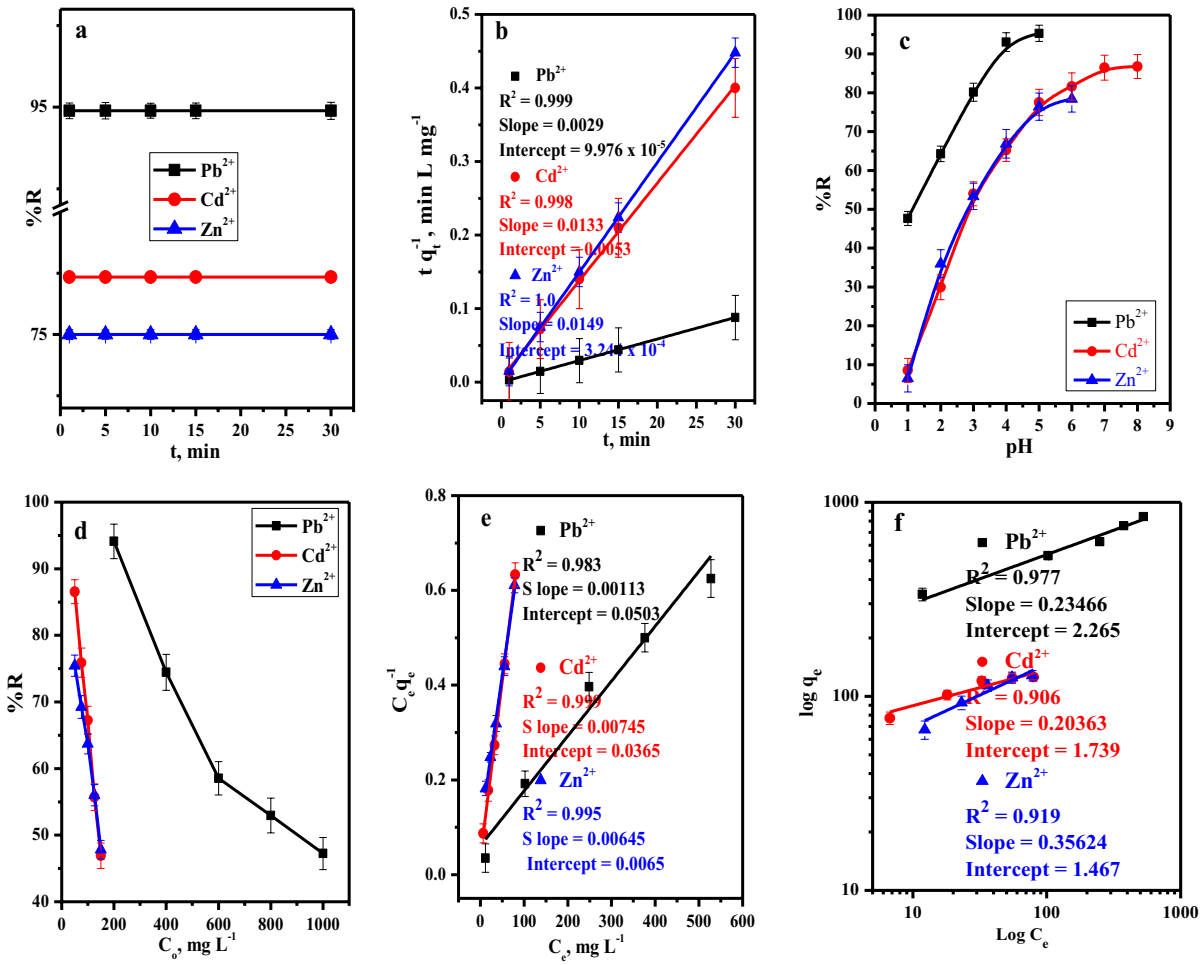

Fig. 4 Effect of **a** contact time on removal percent (%R), **b** 2nd order kinetic model of Pb^{2+} ($[Pb^{2+}]=200$ mg L^{-1}, Dose = 2.8 mg, v = 5 mL, pH = 5, T = 25 °C) Cd^{2+}($[Cd^{2+}]=50$ mg L^{-1}, Dose = 2.8 mg, v = 5 mL, pH = 5, T = 25 °C) and Zn^{2+}($[Zn^{2+}]=50$ mg L^{-1}, Dose = 2.8 mg, v = 5 mL, pH = 5, T = 25 °C) from aqueous media. **c** Effect of the initial solution pH on the removal percentage (% R) from aqueous solution of Pb^{2+}(t = 1 min, $[Pb^{2+}]=200$ mg L^{-1}, Dose = 2.8 mg, v = 5 mL, T = 25 °C) Cd^{2+}(t = 1 min $[Cu^{2+}]=50$ mg L^{-1}, Dose = 2.8 mg, v = 5 mL, T = 25 °C) and Zn^{2+}(t = 1 min, $[Zn^{2+}]=50$ mg L^{-1}, Dose = 2.8 mg, v = 5 mL, T = 25 °C) form aqueous media. **d** metal ion concentration on removal percent, **e** Langmuir isotherm plot, **f** Freundlich isotherm plot of Pb^{2+}(t = 1 min, Dose = 2.8 mg, v = 5 mL, pH = 4, T = 25 °C) Cd^{2+}(t = 1 min, Dose = 2.8 mg, v = 5 mL, pH = 7, T = 25 °C) and Zn^{2+}(t = 1 min, Dose = 2.8 mg, v = 5 mL, pH = 5, T = 25 °C) form aqueous solution

and reached equilibrium within 1.0 min shaking. The highly rapid sorption kinetics of the studied heavy metal ions may refer to either surface complexation or strong chemisorption of these heavy metals on the GO-SA surface (Liu et al. 2015a, b), and the separated layer structure of the GO-SA as appeared in the TEM analysis, see Fig. 1a–c.

To kinetically assess these results, the second-order kinetic equation was applied (see supplementary materials). The results obtained are given in Fig. 4b. The relation coefficient and other parameters were calculated from the linear relation between t and t/q_e and summarized in Table S2. We noted that the $R^2 \geq 0.995$ (close to unit). Moreover, the calculated (q_{cal}, mg g^{-1}) for all tested metal ions were greatly close to the adsorption capacity values measured from experiments (q_{exp}, mg g^{-1}). Therefore, we suggested that the adsorption kinetics followed the pseudo-second-order kinetics model, and the adsorption rate was mainly described via the chemical adsorption process.

Effect of solution pH

In the sorption process, the pH values of the aqueous solution are considered an important factor. Where the variation in the solution pH induces the behavior of adsorbent surface-active groups and the nature of the adsorbate species. Here, we adjusted the pH values according to the nature of heavy metals to avoid precipitation. It was found that the removal efficiency of the GO-SA is high dependence on the pH value of the contaminated solution, see Fig. 4c. At low pH values, the removal efficiency (%R) is relatively low and sharply increases with further increase in the solution pH. This behavior may be attributed to the GO-SA composite possesses carboxylated (COO^-Na^+) groups on its surface, and these groups were responsible for the interaction with the contaminated species. Therefore, at low pH, the concentration of H^+ is high and will block the active adsorption site against the heavy metal. Conversely, by increasing the pH value, the number of the H^+ ion will be minimized, and the surface-active groups (COO^-) become highly ionized, which provides a favorable sorption site for the heavy metal ion (Wang et al. 2016; Huang et al. 2018), see Scheme S1.

Further, the EDS analysis, before and after the adsorption of M-ions (Pb, Cd and Zn) from the aqueous solutions using GO-SA are given in Fig. 3b. From this figure, we observed that, after the adsorption process, there was appearance of Pb, Cd and Zn and absence of Na in the obtained EDS analysis. This result showed that the adsorbed M-ions (Pb, Cd and Zn) substituted the Na from the carboxylate (COO^-Na^+) groups. In addition, the IR spectra of FTIR given in, Fig. S4, showed a new band at 450 cm^{-1}, related to the M–O bond stretching vibration (Małecka and Łącz 2008). Based on the previous observations, it is concluded that the M-ions, Pb, Cd and Zn adsorbed on the GO-SA through cationic exchange mechanism, see Scheme S1.

Effect of initial metal ion concentration

The metal ion concentration plays a vital role in retarding the mass transfer resistance among the aqueous and solid phases (Nurhajawarsi et al. 2018). The influence of the initial metal ion concentration on the removal percent (%R) was studied using the batch approach in rang (200–1000 mg L^{-1}) for Pb^{2+} and (25–150 mg L^{-1}) for Cd^{2+} and Zn^{2+} (Fig. 4d). It is obvious that the GO-SA uptake efficiency decreases with a further increase in the initial concentration of the metal ion. This manner indicates that at a low initial concentration of the metal ions, the number of metal ions is relatively low compared with the number of available active surface functional groups. While at a high initial concentration of metal ions, the number of metal ions will be high compared with the available binding sites at the composite surface. Therefore, the adsorption percent (%R) tends to decrease (Taamneh et al. 2017).

Numerous isotherm models have been employed to fit the experimental results. Among these, Langmuir and Freundlich models are the most applied (see supplementary materials) in order to describe the interaction behavior between the metal ions and the used composite GO-SA (Fig. 4e and f). The calculated parameters and correlation coefficient (R^2) revealed in the used models are listed in Table 1. The R^2 values related to the Langmuir model were > 0.98, which is higher than that of the Freundlich isotherm for all studied metal ions. This result clarifies that the Langmuir model is more suitable for representing the experimental data. Moreover, according to the Langmuir model, the GO-SA composite presents

Table 1 Langmuir and Freundlich constants for adsorption of Pb^{2+}(t = 1 min, Dose = 2.8 mg, v = 5 mL, pH = 4, T = 25 °C) Cd^{2+}(t = 1 min, Dose = 2.8 mg, v = 5 mL, pH = 7, T = 25 °C) and Zn^{2+}(t = 1 min, Dose = 2.8 mg, v = 5 mL, pH = 5, T = 25 °C) form aqueous solution

M^{z+}	q_{exp}, mg g^{-1}	Freundlich parameters			Langmuir parameters			
		K_f, mg g^{-1}	n	R^2	Q_o, mg g^{-1}	b, mL mg^{-1}	R_L	R^2
Pb^{2+}	887.21	184.17	4.26	0.977	884.96	0.018	0.217	0.983
Cd^{2+}	139.62	54.79	4.91	0.906	134.23	0.204	0.089	0.999
Zn^{2+}	161.25	29.27	2.81	0.919	155.04	0.067	0.229	0.995

the maximum adsorption capacities (mg g^{-1}); Pb^{2+} (884.96), Cd^{2+} (134.23), and Zn^{2+} (155.04), see Table 1.

Effect of (v/m) ratio

The effect of changing the v/m (L/g) ratio on the sorption of Pb^{2+} (600 mg L^{-1}), Cd^{2+} (100 mg L^{-1}), and Zn^{2+} (100 mg L^{-1}) from the aqueous solution on GO-SA is performed out at a v/m range of 1.79–0.357 L/g. The obtained results are given in Fig. 5a, from which it is apparent that the sorption efficiency for all studied metal ions decrease with further increase in the v/m ratio. This manner is attributed to the number of the available active sites that are sufficient to adsorb most adsorbate species at a low v/m ratio. As the v/m ratio increases, the number of the metal ion in the solution increases while the number of the binding sites maintain constant. Therefore, many adsorbate species remain in the aqueous solution after the adsorption process; hence, the uptake efficiency will be reduced (Abu Elgoud et al. 2019).

Effect of solution temperature

The impact of aqueous solution temperature (25–65 °C) on the removal percent (%R) of the examined heavy metal ions on the GO-SA composite was presented in Fig. 5b. It was noted that the sorption efficiency of all studied metals was increased with an increase in the solution temperature from 25 to 65 °C. This is due to the increase in the solution temperature will enhance the movement of the metal ion species from the bulk of the solution to the adsorbent surface, leading to an increase in the complexation chance between the metal ion and the surface functional groups.

For exploring the thermodynamic parameters, (see supplementary materials), the adsorption process of the selected metal ions on the GO-SA composite, free energy, entropy, and enthalpy were determined, referring to Fig. 5c. The values of parameters were calculated and listed in Table 2. The negative values of ΔG indicate that all metals studied were spontaneously sorbed on the GO-SA surface. The positive values corresponding to ΔH and ΔS (Table 2) imply the endothermic adsorption process as well as the affinity of the composite to adsorb the metal ion with the increase in the randomness of the system.

Regeneration- reuse

The adsorption–desorption behavior of the adsorbent material is a key index to estimate the suitability of the adsorbent employment in actual sewage management. In this regard, a definite amount of the adsorbent was utilized to adsorb the studied metal ions. After achieving equilibrium, the supernatants were separated, and the %R was calculated. The GO-SA-M material was washed with solutions of 5.0 mL (0.5 M HCl) to remove all sorbed metal ions and regenerate. The composite was then treated with 5.0 mL (0.5 M NaOH) and finally with 5 mL (distilled water) for the next use (see Scheme S1). As presented in Fig. 5d, GO-SA showed excellent reproducibility for adsorbing Pb^{2+}, Cd^{2+}, and Zn^{2+} over five adsorption/desorption experimental runs. However, it is noted that the removal efficiency of the regenerated composite of all studied metal ions was enhanced compared to the original composite. This result may be attributed to the regeneration solutions activating extra binding sites and making them available for adsorption of more metal ions.

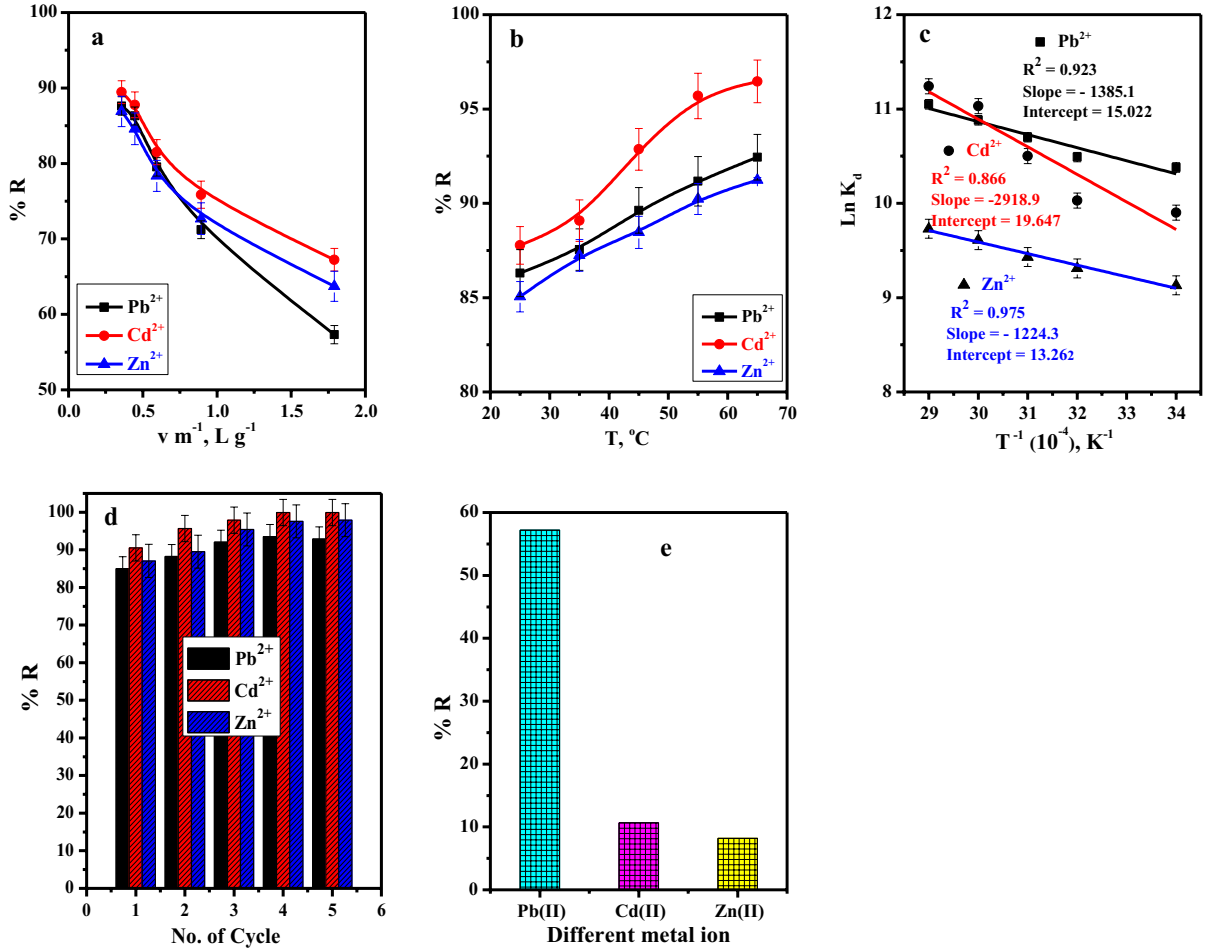

Fig. 5 Effect of **a** v/m ratio on sorption of Pb^{2+} (t = 1 min, [Pb] = 600 mg L^{-1}, v = 5 mL, pH = 4, T = 25 °C), Cd^{2+}(t = 1 min, [Cd] = 100 mg L^{-1},v = 5 mL, pH = 7, T = 25 °C) andCo^{2+}(t = 1 min, [Zn] = 100 mg L^{-1},v = 5 mL, pH = 5, T = 25 °C) form aqueous media. **b** temperature on the removal percent and **c** thermodynamic parameters of Pb^{2+}(t = 1 min, [Pb] = 600 mg L^{-1}, Dose = 11.2 mg, v = 5 mL, pH = 4, T = 25 °C) Cd^{2+}(t = 1 min, [Cd] = 100 mg L^{-1}, Dose = 11.2 mg, v = 5 mL, pH = 7, T = 25 °C) and Zn^{2+}(t = 1 min, [Zn] = 100 mg L^{-1}, Dose = 11.2 mg, v = 5 mL, pH = 5, T = 25 °C) form aqueous solution. **d** the number of the re-use cycles of the GO-C on the removal percentage of Pb^{2+} (t = 1 min, [Pb] = 600 mg L^{-1}, Dose = 14 mg, v = 5 mL, pH = 4, T = 25 °C), Cd^{2+}(t = 1 min, [Cd] = 100 mg L^{-1}, Dose = 14 mg, v = 5 mL, pH = 7, T = 2 °C) and Zn^{2+}(t = 1 min, [Zn] = 100 mg L^{-1}, Dose = 14 mg, v = 5 mL, pH = 5, T = 25 °C) from aqueous media. **e** Selective removal of Pb (II) from metal ion mixture from aqueous solution. [M^{z}+] ([Pb] = 600 mg L^{-1}, [Cd] = 100 mg L^{-1}, [Zn] = 100 mg $L.^{-1}$, v = 10 mL, Dose = 0.014 gm, pH = 1, t = 1 min, T = 25 °C)

Table 2 Thermodynamic parameters for sorption of Pb^{2+}, Cd^{2+} and Zn^{2+} ions

T (K)	ΔG (kJ/mole)			ΔH(kJ/mole)			ΔS (J/mole/K)		
	Pb^{2+}	Cd^{2+}	Zn^{2+}	Pb^{2+}	Cd^{2+}	Zn^{2+}	Pb^{2+}	Cd^{2+}	Zn^{2+}
298	−25.70	−24.41	−22.68						
308	−26.95	−26.04	−23.78						
318	−28.20	−27.68	−24.88	11.52	24.27	10.18	124.89	163.35	110.26
328	−29.44	−29.31	−25.99						
338	−30.69	−30.94	−27.09						

Table 3 Adsorption capacities of different adsorbents of Pb^{2+}, Cd^{2+} and Zn^{2+}

Adsorbate	Adsorbent	q_o(mg/g)	References
Pb^{2+}	(GO–Zr-P) nanocomposite	363.42	Pourbeyram (2016)
	Zinc oxide/graphene oxide nanocomposite	418.78	Ahmad et al. (2020)
	rGO-Fe0/Fe3O4-PEI nanocomposite	60.24	Bagheri et al. (2020)
	Graphene oxide-terminated hyperbranched amino polymer-carboxymethyl cellulose ternary nanocomposite	152.86	Kong et al. (2020)
	Oily sludge pyrolysis residue	140.65	Yang et al. (2020)
	Graphene Oxide/Sodium Alginate/1, 2-Propanediamine composite membrane	189.25	Yu et al. (2021)
	Sodium alginate/graphene oxide aerogel	267.4	Jiao et al. (2016)
	3D porous graphene/lignin/sodium alginate composite	226.24	Zhou et al. (2018)
	A porous calcium alginate/graphene oxide composite aerogel	368.2	Pan et al. (2018)
	EDTA-GO	508.4	Cui et al. (2015)
	Functionalized graphene (GNSPF6)	406.4	Deng et al. (2010)
	GO	35.6	Lee and Yang (2012)
	GO–TiO_2	65.6	Lee and Yang (2012)
	GO-SA	887.21	This work
Cd^{2+}	rGO-Fe0/Fe3O4-PEI nanocomposite	54.47	Bagheri et al. (2020)
	Oily sludge pyrolysis residue	106.16	Yang et al. (2020)
	3D porous graphene/lignin/sodium alginate composite	79.88	Zhou et al. (2018)
	Functionalized graphene (GNSPF6)	73.42	Deng et al. (2010)
	GO	14.9	Lee and Yang (2012)
	GO–TiO_2	72.8	Lee and Yang (2012)
	RGO–Fe(0)/Fe3O4	1.91	Bhunia et al. (2012)
	GO-SA	139.62	This work
Zn^{2+}	GO	30.1	Lee and Yang (2012)
	GO–TiO2	88.9	Lee and Yang (2012)
	Mango peel	28.2	Iqbal et al. (2009)
	Magnetite (MG)	33.95	Abdus Salam and Adekola (2018)
	Baobab fruit shell (BB)	29.20	Abdus Salam and Adekola (2018)
	Magnetite–baobab composite (MB)	38.25	Abdus Salam andAdekola (2018)
	GO-SA	161.25	This work

Selectivity behavior towards Pb^{2+}

Based on the adsorption experiment results, the selectivity of Pb^{2+} adsorption by GO-SA was assessed relative to Cd^{2+} and Zn^{2+}. These metal ions could be considered competitive species during the adsorption of Pb^{2+} from acidic aqueous solution at pH 1 containing Cd^{2+} and Zn^{2+}, as present in Fig. 5e. The affinity of the GO-SA adsorbent towards the tested metal ion in order Pb^{2+} (57.21%) > Cd^{2+} (10.65%) > Zn^{2+} (8.21%) from initial metal ion concentration 600, 100, and 100 mg L^{-1}, respectively. The previous results implied that the GO-SA own an excellent ability to select removal of Pb^{2+} from metal ion mixture solution at pH 1. Based on Pearson's hard/soft acid/base (HSAB) theory, Pb^{2+} could be classified as a softer acid than other metal ions (Cd^{2+} and Zn^{2+}) attributed to its significant water binding energy and higher radius of hydrated ions. On the other hand, the COO– groups act as soft bases in GO-SA, which easily interact with the soft metal Pb^{2+}, resulting in notable selectivity for Pb^{2+} adsorption (Zhou et al. 2022; Ge et al. 2016).

Moreover, the affinity order of GO-SA excellent agreed with the electronegativity of the metal and first stability constant of therelated metal hydroxide

(Dastgheib and Rockstraw 2002). Since, the higher electronegativity of heavy metal ions, the stronger attraction of the heavy metal ions on the negatively charged GO-SA surface. Therefore, the complexation ability of heavy metal species with surface oxygenous functional groups(–COO^-) was also one possible adsorption mode, and the speciation of heavy metal ion species was determined by the stability constants. The above affinity order was very consistent with the first stability constant of the associated metal hydroxide ($Me^{2+} + OH^- \leftrightarrow Me(OH)^+$; log K1 = 7.82, 4.17, 4.4 for $Pb(OH)^+$, $Cd(OH)^+$ and $Zn(OH)^+$, respectively) (Peng et al. 2017).

Comparison with other adsorbent materials

The efficiency of SA modified GO as an adsorbent for removal of Pb^{2+}, Cd^{2+} and $Zn^{2+}$from aqueous solution was estimated by comparing the adsorption capacity with other adsorbent materials in the literature presented in Table 3. The data showed that GO-SA has a highly feasible capacity for the sorption of studied metal ions compared with other adsorbent materials. Therefore, GO-SA composite could be used as a highly effective adsorbent for the removal of these metals from the aqueous solutions.

Conclusion

In this paper we succeeded to modify the GO with highly active biopolymer (SA) through mild conditions. The as-synthesized composite (GO-SA) was characterized by TEM, SEM, FTIR, Raman, TGA and EDX. The activity of the GO-SA was evaluated using batch adsorption process of different heavy metal. Based on the maximum adsorption capacities of the GO-SA the best adsorption conditions towards different metal ions were; Pb^{2+}(t = 1 min, Dose = 2.8 mg, v = 5 mL, pH = 4, T = 25 °C); Cd^{2+}(t = 1 min, Dose = 2.8 mg, v = 5 mL, pH = 7, T = 25 °C) and Zn^{2+}(t = 1 min, Dose = 2.8 mg, v = 5 mL, pH = 5, T = 25 °C). Under these conditions Langmuir isotherm model recorded that, the GO-SA achieve maximum adsorption capacity 887.21, 161.25 and 139.62 mg g^{-1} for Pb^{2+}, Zn^{2+} and Cd^{2+}, respectively. Moreover, the GO-SA represents excellent regeneration ability with enhancing the removal efficiency over five reuse runs. In addition, the GO-SA composite can selectively adsorb Pb^{2+} from low acid of pH = 1.0 in presence of Cd^{2+} and Zn^{2+}.

Funding Open access funding provided by The Science, Technology & Innovation Funding Authority (STDF) in cooperation with The Egyptian Knowledge Bank (EKB). The authors have not disclosed any funding.

Declarations

Conflict of interest The authors have no declarations of interest.

References

Abd-Elhamid AI, Aly HF, Soliman HA, El-Shanshory AA (2018) Graphene oxide: follow the oxidation mechanism and its application in water treatment. J Mol Liq 265:226–237. https://doi.org/10.1016/j.molliq.2018.05.127

Abdus-Salam N, Adekola SK (2018) Adsorption studies of zinc (II) on magnetite, baobab (Adansonia digitata) and magnetite–baobab composite. Appl Water Sci 8(8):1–11

Ablouh EH, Hanani Z, Eladlani N, Rhazi M, Taourirte M (2019) Chitosan microspheres/sodium alginate hybrid beads: an efficient green adsorbent for heavy metals removal from aqueous solutions. Sust Environ Res 29(1):1–11. https://doi.org/10.1186/s42834-019-0004-9

Abu Elgoud EM, Ismail ZH, El-Nadi YA, Abdelwahab SM, Aly HF (2019) Extraction of some rare earth elements (La, Pr and Er) from citrate medium using D2EHPA in kerosene. Arab J Nucl Sci Appl 52:74–85

Aglan RF, Hamed MM (2014) Optimization of environmental friendly process for removal of cadmium from wastewater. Russ J Appl Chem 87(3):373–382. https://doi.org/10.1134/S1070427214030215

Ahmad SZN, Salleh WNW, Yusof N, Yusop MZM, Hamdan R, Awang NA, Ismail NH, Rosman N, Ibrahim H, Ismail AF (2020) Efficient Removal of Pb (II) from aqueous solution using zinc oxide/graphene oxide composite. In: IOP Conference series: material science engineering 736:052002. IOP Publishing. https://doi.org/10.1088/1757-899X/736/5/052002

Ali SA, Ache HJ (1985) Separation and purification of fission products from process streams of irradiated nuclear fuel. Radiochim Acta 40:1

Allouss D, Essamlali Y, Chakir A, Khadhar S, Zahouily M (2020) Effective removal of Cu (II) from aqueous solution over graphene oxide encapsulated carboxymethylcellulose-alginate hydrogel microspheres: towards real wastewater treatment plants. Environ Sci Poll Res 27(7):7476–7492

Bagheri S, Esrafili A, Kermani M, Mehralipour J, Gholami M (2020) Performance evaluation of a novel rGO-Fe0/Fe3O4-PEI nanocomposite for lead and cadmium removal from aqueous solutions. J Mol Liq 320:114422

Bhunia P, Kim G, Baik C, Lee H (2012) A strategically designed porous iron–iron oxide matrix on graphene for heavy metal adsorption. Chem Commun 48(79):9888–9890

Carolin CF, Kumar PS, Saravanan A, Joshiba GJ, Naushad M (2017b) Efficient techniques for the removal of toxic heavy metals from aquatic environment: a review. J Environ Chem Eng 5(3):2782–2799. https://doi.org/10.1016/j.jece.2017.05.029

Carolin CF, Kumar PS, Saravanan A, Joshiba GJ, Naushad M (2017a) Efficient control. In: Proceedings of the 11th international congress of the international radiation protection association, France

Cui L, Wang Y, Gao L, Hu L, Yan L, Wei Q, Du B (2015) EDTA functionalized magnetic graphene oxide for removal of Pb (II), Hg (II) and Cu (II) in water treatment: adsorption mechanism and separation property. Chem Eng J 281:1–10

Dastgheib SA, Rockstraw DA (2002) A model for the adsorption of single metal ion solutes in aqueous solution onto activated carbon produced from pecan shells. Carbon 40(11):1843–1851

Deng X, Lu L, Li H, Luo F (2010) The adsorption properties of Pb(II) and Cd(II) on functionalized graphene prepared by electrolysis method. J Hazard Mater 183:923–930

Dodd B (2020) Safety and security of radioactive sources: conflicts, commonalities and control. Current trends in radiation protection, Les Ulis: EDP Sci 165–176. https://doi.org/10.1051/978-2-7598-0117-6.c016

Febrianastuti S, Fadillah G, Putri ENK, Apriani UW, Wahyuningsih S (2019) Effect of pH $CaCl_2$ solution on graphene oxide encapsulated alginate (GO-AL) for removing methylene blue dyes. IOP Conf Ser Mater Sci Eng 509:012143. https://doi.org/10.1088/1757-899X/509/1/012143

Ge H, Ma Z (2015) Microwave preparation of triethylenetetramine modified graphene oxide/chitosan composite for adsorption of Cr (VI). Carbohydr Polym 131:280–287

Ge H, Hua T, Chen X (2016) Selective adsorption of lead on grafted and crosslinked chitosan nanoparticles prepared by using Pb^{2+}as template. J Hazard Mater 308:225–232

Gopalakannan V, Viswanathan N (2016) One pot synthesis of metal ion anchored alginate–gelatin binary biocomposite for efficient Cr (VI) removal. Int J Biol Macromol 83:450–459

Guo T, Bulin C, Li B, Zhao Z, Yu H, Sun H, Ge X, Xing R, Zhang B (2018) Efficient removal of aqueous Pb (II) using partially reduced graphene oxide-Fe_3O_4. Adsorpt Sci Technol 36(3–4):1031–1048. https://doi.org/10.1177/0263617417744402

He J, Ni F, Cui A, Chen X, Deng S, Shen F, Luo L (2020) New insight into adsorption and co-adsorption of arsenic and tetracycline using a Y-immobilized graphene oxide-alginate hydrogel: adsorption behaviours and mechanisms. Sci Total Environ 701:134363

Huang Y, Wang Z (2018) Preparation of composite aerogels based on sodium alginate, and its application in removal of Pb^{2+} and Cu^{2+} from water. Int J Biol Macromol 107:741–747

Iqbal M, Saeed A, Kalim I (2009) Characterization of adsorptive capacity and investigation of mechanism of Cu2+, Ni2+ and Zn2+ adsorption on mango peel waste from constituted metal solution and genuine electroplating effluent. Sep Sci Technol 44(15):3770–379. https://doi.org/10.1080/01496390903182305

Jiao C, Xiong J, Tao J, Xu S, Zhang D, Lin H, Chen Y (2016) Sodium alginate/graphene oxide aerogel with enhanced strength–toughness and its heavy metal adsorption study. Int J Biol Macromol 83:133–141. https://doi.org/10.1016/j.ijbiomac.2015.11.061

Katubi KMM, Alsaiari NS, Alzahrani FM, Siddeeg SM, Tahoon MA (2021) Synthesis of manganese ferrite/graphene oxide magnetic nanocomposite for pollutants removal from water. Processes 9(4):589. https://doi.org/10.3390/pr9040589

Kong Q, Preis S, Li L, Luo P, Hu Y, Wei C (2020) Graphene oxide-.for efficient removal of heavy metals from aqueous solutions. Int J Biol Macromol 149:581–592. https://doi.org/10.1016/j.ijbiomac.2020.01.185

Lee YC, Yang JW (2012) Self-assembled flower-like TiO_2 on exfoliated graphite oxide for heavy metal removal. J Ind Eng Chem 18(3):1178–1185

Li L, Zhao L, Ma J, Tian Y (2020) Preparation of graphene oxide/chitosan complex and its adsorption properties for heavy metal ions. Green Proc Syn 9(1):294–303. https://doi.org/10.1515/gps-2020-0030

Liu X, Li J, Wang X, Chen C, Wang X (2015a) High performance of phosphate- functionalized graphene oxide for the selective adsorption of U (VI) from acidic solution. J Nucl Mater 466:56–64. https://doi.org/10.1016/j.jnucmat.2015.07.027

Liu Y, Zhao JC, Zhang CJ, Guo Y, Cui L, Zhu P, Wang DY (2015b) Bio- based nickel alginate and copper alginate films with excellent flame retardancy: preparation, flammability and thermal degradation behavior. RSC Adv 5(79):64125–64137

Małecka B, Łącz A (2008) Thermal decomposition of cadmium format in inert and oxidative atmosphere. Thermochim Acta 479(1–2):12–16. https://doi.org/10.1016/j.tca.2008.09.003

Marczenko Z (1976) Spectrophotometric determination of elements. Ellis Harwood Ltd, Poland

Nigiz FU (2020) Graphene oxide-sodium alginate membrane for seawater desalination through pervaporation. Desalination 485:114465. https://doi.org/10.1016/j.desal.2020.114465

Nurhajawarsi N, Rafi M, Syafitri UD, Rohaeti E (2018) L-histidine-modified silica from rice husk and optimization of

adsorption condition for extractive concentration of Pb (II). J Pure Appl Chem Res 7(2):198

Pan L, Wang Z, Yang Q, Huang R (2018) Efficient removal of lead, copper and cadmium ions from water by a porous calcium alginate/graphene oxide composite aerogel. Nanomaterials 8(11):957. https://doi.org/10.3390/nano8110957

Peng W, Li H, Liu Y, Song S (2017) A review on heavy metal ions adsorption from water by graphene oxide and its composites. J Mol Liq 230:496–504

Pourbeyram S (2016) Effective removal of heavy metals from aqueous solutions by graphene oxide–zirconium phosphate (GO–Zr-P) nanocomposite. Ind Eng Chem Res 55(19):5608–5617. https://doi.org/10.1021/acs.iecr.6b00728

Rodríguez C, Tapia C, Leiva-Aravena E, Leiva E (2020) Graphene oxide–ZnO nanocomposites for removal of aluminum and copper ions from acid mine drainage wastewater. Int J Environ Res Public Health 17(18):6911. https://doi.org/10.3390/ijerph17186911

Taamneh Y, Sharadqah S (2017) The removal of heavy metals from aqueous solution using natural Jordanian zeolite. Appl Water Sci 7(4):2021–2028

Wang Z, Huang Y, Wang M, Wu G, Geng T, Zhao Y, Wu A (2016) Macroporous calcium alginate aerogel as sorbent for Pb^{2+} removal from water media. J Environ Chem Eng 4(3):3185–3192

Yang H, Li Z, Ma W, Fu P (2020) Evaluation of pyrolysis residue derived by oily sludge on removing heavy metals from artificial flotation wastewater. S Afr J Chem Eng 34:82–89. https://doi.org/10.1016/j.sajce.2020.06.005

Yu Y, Zhang G, Ye L (2019) Preparation and adsorption mechanism of polyvinyl alcohol/graphene oxide-sodium alginate nanocomposite hydrogel with high Pb (II) adsorption capacity. J Appl Pol Sci 136(14):47318

Yu Y, Sun R, Wang Z, Yao M, Wang G (2021) Self-supported Graphene Oxide/Sodium Alginate/1, 2-Propanediamine composite membrane and its Pb^{2+} adsorption capability. J Environ Chem Eng 9(5):106254

Zhou F, Feng X, Yu J, Jiang X (2018) High performance of 3D porous graphene/lignin/sodium alginate composite for adsorption of Cd (II) and Pb (II). Environ Sci Poll Res 25(16):15651–15661. https://doi.org/10.1007/s11356-018-1733-8

Zhou X, Liu Y, Jin C, Wu G, Liu G, Kong Z (2022) Efficient and selective removal of Pb (II) from aqueous solution by a thioether-functionalized lignin-based magnetic adsorbent. RSC Adv 12:1130